IEEE Access
Multidisciplinary | Rapid Review | Open Access Journal

Received June 20, 2020, accepted July 3, 2020, date of publication July 6, 2020, date of current version July 17, 2020.

Digital Object Identifier 10.1109/ACCESS.2020.3007505

Theoretical Investigation of Radiation in the Normal Direction for a Metaloop Antenna

HISAMATSU NAKANO, (Life Fellow, IEEE), TOMOKI ABE, (Member, IEEE), AND JUNJI YAMAUCHI, (Life Fellow, IEEE)
Department of Science and Engineering, Hosei University, Tokyo 184-8584, Japan
Corresponding author: Hisamatsu Nakano (hymat@hosei.ac.jp)

This work was supported in part by the Japan Society for the Promotion of Science (JSPS) KAKENHI under Grant JP18K04154.

ABSTRACT Radiation in the normal direction for a metaloop antenna is discussed. First, the radiation field generated from an N-type current distributed along a loop, $\mathbf{E}_{\mathrm{N}}$, is investigated. The investigation clarifies the behavior of the unbalance between the left-handed circularly polarized (LHCP) component of $\mathbf{E}_{\mathrm{N}}$ at frequency $f_{(-)}$ and the right-handed circularly polarized (RHCP) component of $\mathbf{E}_{\mathrm{N}}$ at frequency $f_{(+)}$, where the loop circumference at these frequencies is one guided wavelength. Secondly, the radiation field generated from a C-type current, $\mathbf{E}_{\mathrm{C}}$, is investigated. The second investigation, when combined with the first investigation, leads to an inference that balanced radiation (and hence balanced gain) will be obtained when the N-type current over a certain region of the loop is replaced with a C-type current. Thirdly, to check this inference, a radiation field generated from a composite of the N-type and C-type currents, $\mathbf{E}_{\mathrm{NC}}$, is formulated. Using this formulation, the ratio of the gain for an LHCP wave to the gain for an RHCP wave, G_{r}, is derived. Fourthly, a metaloop antenna simulation model that has a balanced gain is created using practical N-type and C-type metaatoms that realize the composite current. Finally, a metaloop antenna is fabricated on the basis of the antenna simulation model. Measurements confirm that the fabricated metaloop antenna has a balanced gain in the normal direction. As supplementary data, the radiation pattern and VSWR of the fabricated metaloop antenna are also presented, together with the radiation efficiency and some comments.

INDEX TERMS Antenna, circularly polarized radiation, gain, metaatoms.

I. INTRODUCTION

Circularly polarized (CP) antennas have been used, for example, in satellite communications and mobile communications and offer the advantage that polarization alignment of the transmitting and receiving antennas is not needed. So far, numerous CP antennas have been proposed [1], [2]. Among these, the axial mode helical antenna in [3]–[6], the spiral antenna in [7]–[9], and the curl antenna in [10]–[12] have become well-known CP antennas.

A loop antenna is an antenna that radiates a linearly polarized (LP) wave [13], [14]. A paper in [15] has revealed that LP radiation can be changed to CP radiation by adding perturbation elements to the loop. Using such a perturbation technique, a C-shaped CP loop antenna has been created [16] and deployed on actual satellites, including mu-LAbSat, SOHLA A-1, and SOCRATES H-II.

The abovementioned helical, spiral, curl, and loop CP antennas are summarized in terms of the antenna height and polarization as follows: (i) they have a ground plane and the antenna height above the ground plane exceeds 1/10 wavelength. (ii) the radiated wave is *either* left-handed circularly polarized (LHCP) or right-handed circularly polarized (RHCP), subject to the winding sense of the antenna arms, *i.e.*, the radiated wave has a single polarization. Such a single polarization characteristic comes from the fact that the propagation phase constant of the current along the antenna arm is positive ($\beta > 0$). Conventional helical, spiral, and curl antennas with currents having only a positive β are categorized as natural antennas.

In contrast, a recently created metaloop antenna has a low-profile structure, where the antenna height is on the order of 1/100 wavelength, and radiates *both* an LHCP wave and an

The associate editor coordinating the review of this manuscript and approving it for publication was Shah Nawaz Burokur.

RHCP wave (counter CP radiation or Cnt-CP radiation) [17]. The Cnt-CP radiation is obtained in two distinct frequency bands (dual-band operation, Du-BND operation). Therefore, we can create a communication system where the interference between transmitting and receiving signals is effectively eliminated. Note that the metaloop antenna has a current with a negative propagation phase constant ($\beta < 0$) across a specific frequency band, and a current with a positive propagation phase constant ($\beta > 0$) across a different frequency band, and is categorized as a metamaterial antenna [18]–[21].

However, as will be clarified in this paper, the metaloop antenna has the drawback that the maximum intensity of the LHCP and RHCP radiation fields in the direction normal to the loop plane is generally not the same, and hence the gain of the Du-BND Cnt-CP radiation in the normal direction is unbalanced. To realize a balanced gain, an amplifier or an attenuator is needed, resulting in high cost and an increase in the complexity of the design of the CP communication system.

So far there has been neither theoretical realization of balanced field intensity in the normal direction nor its experimental demonstration [22]–[25], except for [26]. The antenna structure in [26] is composed of a square metaloop antenna and a square parasitic loop placed above the metaloop antenna, thereby realizing a balanced gain. Note that such a solution leads to a high profile structure; in other words, the advantage of a low-profile structure of the metaloop antenna itself disappears.

Most recent numerical analysis [27] has quasi-theoretically shown the behavior of the polarization and field intensity in the normal (broadside) direction of metaloop antennas (RND-MTLP-C, RND-MTLP-N, SQR-MTLP-C, SQR-MTLP-N). However, it has not referred to any solutions to balancing the field intensities in Du-BND Cnt-CP radiation.

This paper resolves the issue of unbalanced radiation field intensities (and hence gains) in the normal direction for the metaloop antenna that is encountered with Du-BND Cnt-CP radiation. To do this, radiation fields $\mathbf{E}_{\mathrm{N}}$, $\mathbf{E}_{\mathrm{C}}$, and $\mathbf{E}_{\mathrm{NC}}$ generated from the respective traveling currents flowing along the loop, $\mathbf{I}_{\mathrm{N}}$, $\mathbf{I}_{\mathrm{C}}$, and $\mathbf{I}_{\mathrm{NC}}$, are formulated. Based on an insight into these radiation fields, an innovative metaloop antenna with a balanced gain is created. The created antenna is called the *NC*-type metaloop antenna, where *N*-type and *C*-type currents are introduced into an antenna design equation for the first time. Note that conventional metaloop antennas, summarized in [27], use either an *N*-type current or a *C*-type current and encounter unbalanced fields in the normal direction.

Six sections constitute this paper, where the discussions in Sections II through IV are, for convenience, referred to as the *preliminary discussions* and prepare for the realization of the targeted metaloop antenna with balanced gain.

Section II considers a situation where an *N*-type current with polarization factor q ($0 \leq q \leq 1$) flows along a loop and generates a radiation field of $\mathbf{E}_{\mathrm{N}}$. We focus on $\mathbf{E}_{\mathrm{N}}$ in the normal direction of the plane of the loop when the circumference is one guided wavelength ($1\lambda_{\mathrm{g}}$), and discuss the effect of q on the LHCP and RHCP radiation field components of $\mathbf{E}_{\mathrm{N}}$. The degree of unbalance between the LHCP and RHCP radiation field components is clarified using q.

Section III discusses a situation where a *C*-type current flows along a loop. We formulate the radiation field in the normal direction, $\mathbf{E}_{\mathrm{C}}$. Based on an insight into $\mathbf{E}_{\mathrm{C}}$ together with the above-mentioned $\mathbf{E}_{\mathrm{N}}$, an inference for obtaining a balanced gain is made. Subsequently, this inference is theoretically (numerically) investigated in Section IV, where the *N*-type current on a certain region of the loop is replaced with a *C*-type current, resulting in a composite of *N*-type and *C*-type currents. The radiation field in the normal direction generated from the composite current, $\mathbf{E}_{\mathrm{NC}}$, is derived. Using $\mathbf{E}_{\mathrm{NC}}$, the behavior of the antenna gain is investigated as a function of the boundary azimuth angle, N_{s} (azimuth angle at the connection point of the *N*-type and *C*-type currents).

Based on the preliminary discussions, Section V presents metaloop antenna simulation models, where practical *N*-type and *C*-type metaatoms that produce corresponding *N*-type and *C*-type currents are introduced. Using the formulas derived in the preliminary discussions together with the simulated results of the antenna models, an innovative metaloop antenna, called the *NC*-type metaloop antenna, is designed such that it has a balanced gain. Finally, the designed *NC*-type metaloop antenna is fabricated and the balanced gain is confirmed by experiment. As supplementary data, simulated and experimental results for the radiation pattern and VSWR of the *NC*-type metaloop antenna are presented, together with the radiation efficiency and some comments. Section VI summarizes the findings obtained in this paper.

It should be emphasized that a challenging point in this paper is the determination of boundary azimuth angle N_{s} for the created *NC*-type metaloop antenna. It is worthy to describe that the determination of N_{s} in this paper is theoretically performed on the basis of newly derived equations and an insight into them; in addition, experiment validates a balanced gain for the *NC*-type metaloop antenna with determined N_{s} for the first time. Thus, the issue of the unbalance gain is resolved.

II. RADIATION FROM AN N-TYPE CURRENT IN THE NORMAL DIRECTION

Fig. 1 shows a loop of radius r_{c}. We assume that a traveling current, $\mathbf{I}_{\mathrm{N}}(s')$, designated as the *N*-type current, is distributed across an angular range of N_{s} to N_{e} [rad] of the loop:

$$\mathbf{I}_{\mathrm{N}}(s') = i_0(\hat{s} - jq\hat{t})e^{-j\beta s'}, \tag{1}$$

where s' is the distance to a current element along the loop measured from point X_{s}, and is called the source point coordinate; i_0 is the amplitude of the current and assumed to be constant; $\hat{s}$ is the unit vector tangential to the loop, and $\hat{t}$ is the unit vector normal to $\hat{s}$; q is a constant ($0 \leq q \leq 1$), called the polarization factor; β is the propagation phase constant, *i.e.*, $\beta = -2\pi/\lambda_g$ for $\beta < 0$ and $\beta = +2\pi/\lambda_g$ for $\beta > 0$ with λ_g being the guided wavelength at frequency f. The phase

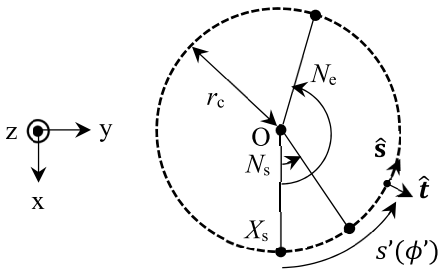

FIGURE 1. *N*-type current distribution.

constants for $\beta < 0$ and $\beta > 0$ are designated as the left-handed phase constant (LH-PhsC) and right-handed phase constant (RH-PhsC), respectively.

Using the rectangular coordinate system of (x, y, z) with unit vectors $(\hat{x}, \hat{y}, \hat{z})$, the unit vectors of $\hat{s}$ and $\hat{t}$ at the source point specified by s' are expressed as

$$\hat{s} = -\sin\phi'\hat{x} + \cos\phi'\hat{y} \tag{2}$$
$$\hat{t} = \cos\phi'\hat{x} + \sin\phi'\hat{y}, \tag{3}$$

where ϕ' is the azimuth angle at the source point on the x-y plane. The radiation field generated by the N-type current at a far-field point of (r, θ, ϕ) (called the observation point), $\mathbf{E}_N$, is expressed as

$$\mathbf{E}_N(r, \theta, \phi) = -ji_0 \frac{\mu\omega}{4\pi r} e^{-jk_0 r} \int_{r_c N_s}^{r_c N_e} \mathbf{P}_{st} e^{-j\beta s'} e^{jk_0 \hat{r}\cdot\mathbf{r}'} ds', \tag{4}$$

where $\mathbf{P}_{st} = \hat{s} - jq\hat{t}$; μ is the permeability in free space; ω $(=2\pi f)$ is the operating angular frequency; k_0 is the propagation phase constant in free space; $\mathbf{r}'$ is the vector directed from the coordinate origin to the source point specified by s'; and $\hat{r}$ is the unit vector directed from the coordinate origin to the observation point.

Our interest is in the radiation field in the direction normal to the loop (in the z-direction), *i.e.,* $\mathbf{E}_N(r, \theta = 0, \phi)$. In this case, the inner product of $(\hat{r} \cdot \mathbf{r}')$ is zero and Eq. (4) at frequency f is expressed as

$$\mathbf{E}_N(r, \theta = 0^o, \phi) = Uf\mathbf{Q}_{LH}\sigma_{stLH} + Uf\mathbf{Q}_{RH}\sigma_{stRH}, \tag{5}$$

where

$$U = -j\frac{\mu}{2r} e^{-jk_0 r} i_0 r_c \tag{6}$$
$$\mathbf{Q}_{LH} = \frac{1+q}{2}(-j\hat{x} + \hat{y}) \tag{7}$$
$$\mathbf{Q}_{RH} = \frac{1-q}{2}(j\hat{x} + \hat{y}) \tag{8}$$
$$\begin{aligned}\sigma_{stLH} &= \int_{N_s}^{N_e} e^{-j(1+\beta r_c)\phi'} d\phi' \\ &= \frac{e^{-j(1+n)N_e} - e^{-j(1+n)N_s}}{-j(1+n)} \\ &\equiv \sigma_{stLH}(n)\end{aligned} \tag{9}$$
$$\begin{aligned}\sigma_{stRH} &= \int_{N_s}^{N_e} e^{j(1-\beta r_c)\phi'} d\phi' \\ &= \frac{e^{j(1-n)N_e} e^{j(1-n)N_s}}{j(1-n)} \\ &\equiv \sigma_{stRH}(n).\end{aligned} \tag{10}$$

The βr_c in Eqs. (9) and (10) is replaced by n, *i.e.*, $\beta r_c = n$, which is negative for $\beta < 0$ and positive for $\beta > 0$. The absolute value of n, $|n|$, is the circumference of the loop of radius r_c normalized to the guided wavelength λ_g at a particular frequency f, and hence $|n|$ is called the normalized circumference. Note that the terms involving $\mathbf{Q}_{LH}$ and $\mathbf{Q}_{RH}$ in Eq. (5) are the LHCP and RHCP radiation field elements of $\mathbf{E}_N$, respectively. Also note that an antenna using the N-type current is called the N-type metaloop antenna, which appears later in Section V.

A. E_N FOR A LEFT-HANDED PHASE CONSTANT (LH-PhsC)

We denote $\mathbf{E}_N(r, \theta = 0, \phi)$ for a phase constant of $\beta < 0$ at frequency $f = f_{(-)}$ as $\mathbf{E}_N^{(-)}(r, \theta = 0, \phi)$. Fig. 2(a) shows the LHCP and RHCP radiation field components of $\mathbf{E}_N^{(-)}(r, \theta = 0, \phi)$, denoted as EN(−) LHCP and EN(−) RHCP, respectively. These components are calculated as a function of normalized circumference n [*i.e.*, $n = \beta r_c = -2\pi r_c/\lambda_g < 0$ with r_c being the loop radius (varied)], with polarization factor q as a parameter.

The condition used here is that the N-type current is distributed *entirely* along the loop with $(N_s, N_e) = (0, 2\pi)$ [rad]. The LHCP and RHCP radiation field components of $\mathbf{E}_N^{(-)}$ are normalized to a value of $|Uf_{(-)}(1+q)\sigma_{stLH}(n)/2|$ for $n = -1$ with $q = 1$:

$$20\log\{|Uf_{(-)}\frac{1+q}{2}\sigma_{stLH}(n)|/|Uf_{(-)}\sigma_{stLH}(-1)|\}\ [\text{dB}]$$
$$\text{for the LHCP radiation field component} \tag{11}$$
$$20\log\{|Uf_{(-)}\frac{1-q}{2}\sigma_{stRH}(n)|/|Uf_{(-)}\sigma_{stLH}(-1)|\}\ [\text{dB}]$$
$$\text{for the RHCP radiation field component.} \tag{12}$$

Hereafter, $|Uf_{(-)}\sigma_{stLH}(-1)|$ is used to normalize the radiation field components, unless otherwise noted. It is found that the principal radiation field component at $f_{(-)}$ is LHCP. The RHCP radiation field component is extremely small: less than −20 dB, except for $q = 0$.

It is worth mentioning that radiation field $\mathbf{E}_N^{(-)}$ for $n = -1$ is always LHCP, regardless of the value of polarization factor q $(0 \le q \le 1)$. This is clarified by reducing Eq. (5) to

$$\mathbf{E}_N^{(-)}(\mathrm{r}, \theta = 0, \phi) = Uf_{(-)}(1+q)\pi\left(-j\hat{x} + \hat{y}\right)$$
$$\text{for } n = -1, \quad \text{with } (N_s, N_e) = (0, 2\pi)\ [\text{rad}], \tag{13}$$

where the following results obtained from Eqs. (9) and (10) are used:

$$\begin{aligned}\sigma_{stLH}(-1) &= N_e - N_s \\ &= 2\pi \quad \text{for } n = -1\end{aligned} \tag{14}$$
$$\begin{aligned}\sigma_{stRH}(-1) &= \frac{e^{j2N_e} - e^{j2N_s}}{j2} \\ &= 0 \quad \text{for } n = -1.\end{aligned} \tag{15}$$

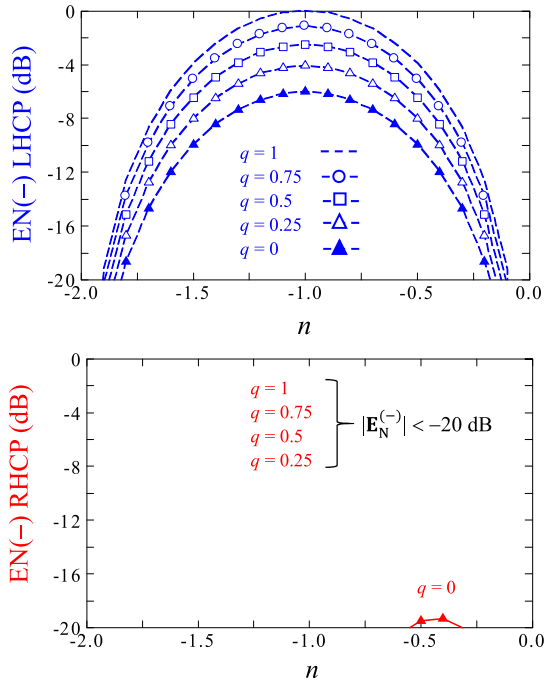

(a)

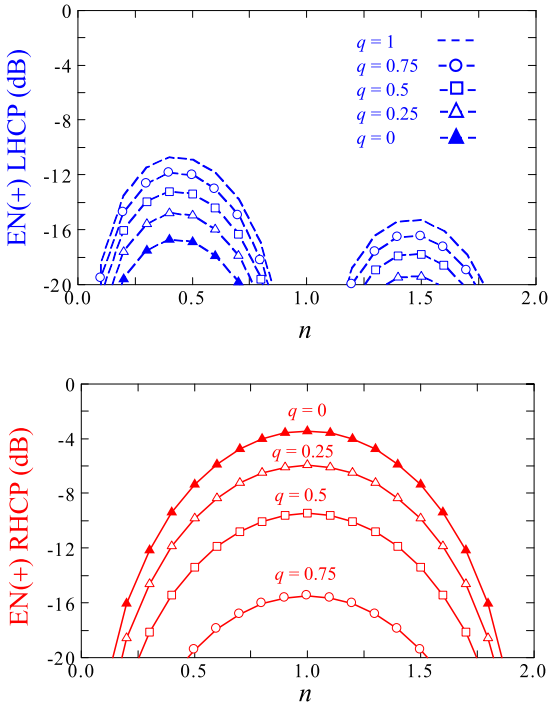

(b)

FIGURE 2. Radiation field $\mathbf{E}_{\mathrm{N}}(r, \theta = 0, \phi)$ as a function of normalized circumference n with polarization factor q as a parameter, where $n = \beta r_{\mathrm{c}}$. (a) $n < 0$, where $\beta < 0$. (b) $n > 0$, where $\beta > 0$.

As the polarization factor is increased to one ($q = 1$), the LHCP radiation field component of Eq. (13) increases.

B. E_N FOR A RIGHT-HANDED PHASE CONSTANT (RH-PhsC)

This subsection investigates the behavior of Eq. (5) for $\beta > 0$ at frequency $f = f_{(+)}$, denoted as $\mathbf{E}_{\mathrm{N}}^{(+)}(r, \theta = 0, \phi)$, where the N-type current is distributed along the entire loop, as in subsection *A*. Fig. 2(b) shows $\mathbf{E}_{\mathrm{N}}^{(+)}(r, \theta = 0, \phi)$ as a function of normalized circumference n ($=\beta r_{\mathrm{c}} = 2\pi r_{\mathrm{c}}/\lambda_{\mathrm{g}} > 0$) with polarization factor q as a parameter, where $f_{(+)} = f_{(-)}/f_{\mathrm{r}}$ is used with a frequency ratio of $f_{\mathrm{r}} = 0.743$, as an example. The basis for f_{r} will be clarified later in Fig. 10.

The two notations of the vertical axis in Fig. 2(b), EN(+) LHCP and EN(+) RHCP, represent the LHCP and RHCP radiation field components of $\mathbf{E}_{\mathrm{N}}^{(+)}(r, \theta = 0, \phi)$, respectively. It is found that the maximum RHCP radiation field component appears when $n = +1$ with $q = 0$. This is numerically understood by reducing Eq. (5)

$$\mathbf{E}_{\mathrm{N}}^{(+)}(r, \theta = 0, \phi) = U f_{(+)}(1 - q)\,\pi\left(j\hat{x} + \hat{y}\right) \quad \text{for } n = +1, \text{ with } (N_{\mathrm{s}}, N_{\mathrm{e}}) = (0, 2\pi) \text{ [rad]}, \tag{16}$$

which is obtained using Eqs. (17) and (18), derived from Eqs. (9) and (10), respectively:

$$\sigma_{\mathrm{stLH}}(+1) = 0 \quad \text{for } n = +1 \tag{17}$$

$$\sigma_{\mathrm{stRH}}(+1) = N_{\mathrm{e}} - N_{\mathrm{s}} = 2\pi \quad \text{for } n = +1. \tag{18}$$

Eq. (16) reveals that, as *the polarization factor* is increased, the RHCP radiation field component decreases and becomes zero when the polarization factor is one ($q = 1$). The unbalance between the RHCP radiation field component for $n = +1$ and the LHCP radiation field component for $n = -1$ becomes maximum when $q = 1$.

C. POLARIZATION FACTOR q AND UNBALANCED RADIATION

Polarization factor q for the N-type current can be obtained using two radiation fields for $(N_{\mathrm{s}}, N_{\mathrm{e}}) = (0, 2\pi)$ [rad]: one is the LHCP radiation field component for $n = -1$ and the other is the RHCP radiation field component for $n = +1$. As described in subsections *A* and *B*, $\mathbf{E}_{\mathrm{N}}^{(-)}$ for $n = -1$ has only an LHCP radiation field component, as seen from Eq. (13); on the other hand, $\mathbf{E}_{\mathrm{N}}^{(+)}$ for $n = +1$ has only an RHCP radiation field component, as seen from Eq. (16). It follows that the gain ratio of the LHCP radiation field component to the RHCP radiation field component, G_{r}, is given as

$$G_{\mathrm{r}} = \left|\frac{\mathrm{EN}\,(-)\,\mathrm{LHCP}}{\mathrm{EN}\,(+)\,\mathrm{RHCP}}\right|^2 = \left|\frac{f_{(-)}\,(1+q)}{f_{(+)}\,(1-q)}\right|^2 \quad \text{for } |n| = 1. \tag{19}$$

From Eq. (19),

$$q = \frac{\sqrt{G_{\mathrm{r}}} - f_{\mathrm{r}}}{\sqrt{G_{\mathrm{r}}} + f_{\mathrm{r}}} \quad \text{for } |n| = 1. \tag{20}$$

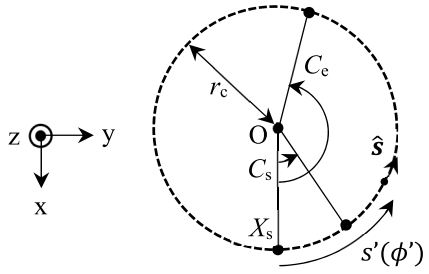

FIGURE 3. *C*-type current distribution.

A balanced gain is obtained when $G_r = 1$. For example, a balanced gain for a frequency ratio of $f_r = f_{(-)}/f_{(+)} = 0.743$ is realized with a polarization factor of $q = 0.147$, which is calculated from Eq. (20). Note that, in reality, it is very difficult to precisely create such a small polarization factor for the N-type metaloop antenna. Therefore, we propose a different technique for gain balancing later in Section V, where a C-type current is introduced across a certain region of the loop. In preparation, we investigate radiation from the C-type current in the following section.

III. RADIATION FROM A C-TYPE CURRENT IN THE NORMAL DIRECTION

We assume a traveling current, $\mathbf{I}_c(s')$, which flows across an angle range of C_s to C_e [rad] on a loop of radius r_c, as shown in Fig. 3.

$$\mathbf{I}_c(s') = i_0 \hat{s} e^{-j\beta s'}. \tag{21}$$

This current is distinct from the N-type current of Eq. (1) and is designated as the C-type current.

The radiation field in the z-direction generated from the C-type current, $\mathbf{E}_C(r, \theta = 0, \phi)$, is derived through the same process used for deriving radiation field $\mathbf{E}_N$:

$$\mathbf{E}_C(r, \theta = 0, \phi) = Uf\mathbf{Q}, \tag{22}$$

where

$$\mathbf{Q} = -\sigma_x \hat{x} + \sigma_y \hat{y} \tag{23}$$

$$\sigma_x = \int_{C_s}^{C_e} \sin\phi' e^{-jn\phi'} d\phi' \tag{24}$$

$$\sigma_y = \int_{C_s}^{C_e} \cos\phi' e^{-jn\phi'} d\phi'. \tag{25}$$

U and n in the above equations have already been defined in Section II. The third element on the right side of Eq. (22) yields

$$\mathbf{Q} = \frac{1}{2} \cdot \frac{e^{j(1-n)C_e} - e^{j(1-n)C_s}}{j(1-n)} \left(j\hat{x} + \hat{y}\right) + \frac{1}{2} \cdot \frac{e^{-j(1+n)C_e} - e^{-j(1+n)C_s}}{-j(1+n)} \left(-j\hat{x} + \hat{y}\right). \tag{26}$$

All results coincide with the previous results for $q = 0$ in Section II.

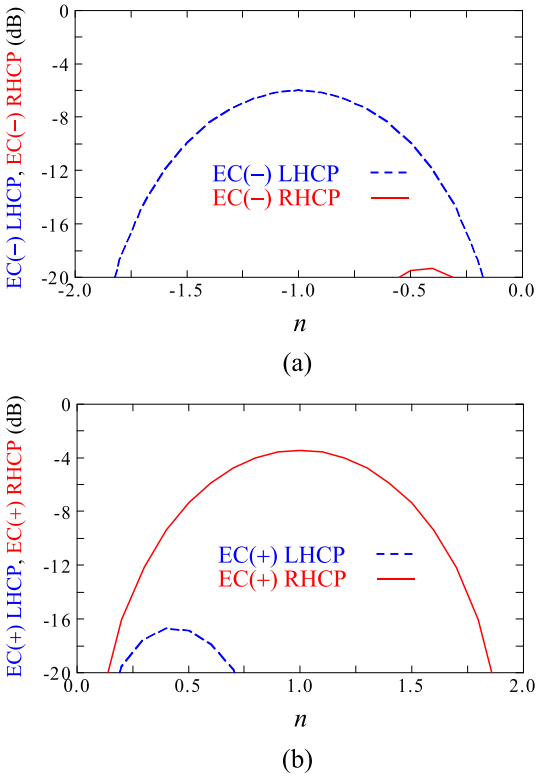

FIGURE 4. Radiation field $\mathbf{E}_C(r, \theta = 0, \phi)$ as a function of normalized circumference n. (a) At $f_{(-)}$. (b) At $f_{(+)}$.

A. E_C FOR A LEFT-HANDED PHASE CONSTANT (LH-PhsC)

Fig. 4(a) shows the radiation field of Eq. (22) at frequency $f_{(-)}$, $\mathbf{E}_C^{(-)}$, as a function of normalized circumference n, with $(C_s, C_e) = (0, 2\pi)$ [rad]. $\mathbf{E}_C^{(-)}$ is decomposed into the LHCP radiation field component, EC(−) LHCP, and the RHCP radiation field component, EC(−) RHCP. It is found that the principal radiation field component is LHCP. The LHCP radiation field component for $n = -1$ reaches its maximum value with the following $\mathbf{Q}$:

$$\mathbf{Q} = \pi \left(-j\hat{x} + \hat{y}\right) \quad \text{for } n = -1, \text{ with } (C_s, C_e) = (0, 2\pi) \text{ [rad]}, \tag{27}$$

which is obtained by applying an angle range of (C_s, C_e) to Eq. (28)

$$\mathbf{Q} = \frac{1}{2} \cdot \frac{e^{j2C_e} - e^{j2C_s}}{j2} \left(j\hat{x} + \hat{y}\right) + \frac{1}{2} \cdot (C_e - C_s) \left(-j\hat{x} + \hat{y}\right) \quad \text{for } n = -1. \tag{28}$$

Eq. (28) is a reduced form of Eq. (26) for $n = -1$.

B. E_C FOR A RIGHT-HANDED PHASE CONSTANT (RH-PhsC)

Fig. 4(b) shows Eq. (22) at frequency $f_{(+)}$, denoted as $\mathbf{E}_C^{(+)}$, where $(C_s, C_e) = (0, 2\pi)$ [rad]. The horizontal axis of this figure is the normalized circumference, n (>0). The notations EC(+) LHCP and EC(+) RHCP are the LHCP and RHCP

radiation field components of $\mathbf{E}_{\mathrm{C}}^{(+)}$, respectively. It is found that the LHCP radiation field component is small and the principal radiation field component is RHCP, whose maximum value is calculated from Eq. (22) with

$$\mathbf{Q} = +\frac{1}{2}\cdot(C_{\mathrm{e}}-C_{\mathrm{s}})\left(j\hat{x}+\hat{y}\right) + \frac{1}{2}\cdot\frac{e^{-j2C_{\mathrm{e}}}-e^{-j2C_{\mathrm{s}}}}{-j2}\left(-j\hat{x}+\hat{y}\right) \quad \text{for } n=+1, \tag{29}$$

which is reduced to

$$\mathbf{Q} = \pi\left(j\hat{x}+\hat{y}\right) \quad \text{for } n=+1, \quad \text{with } (C_{\mathrm{s}}, C_{\mathrm{e}}) = (0, 2\pi)\ [\mathrm{rad}]. \tag{30}$$

In summary, the $\mathbf{E}_{\mathrm{C}}$ for a $1\lambda_{\mathrm{g}}$-circumference loop (normalized circumference $|n|=1$) has the following characteristic: the maximum LHCP radiation field component at $f_{(-)}$ for $\beta<0$ is smaller than the maximum RHCP radiation field component at $f_{(+)}$ for $\beta>0$. Correspondingly, the gain for an LHCP wave (G_{LHCP}) at $f_{(-)}$ for $\beta<0$ is smaller than the gain for an RHCP wave (G_{RHCP}) at $f_{(+)}$ for $\beta>0$: $G_{\mathrm{LHCP}}<G_{\mathrm{RHCP}}$. This is in contrast to the $\mathbf{E}_{\mathrm{N}}$ for a $1\lambda_{\mathrm{g}}$-circumference loop (normalized circumference $|n|=1$): the LHCP radiation field component of $\mathbf{E}_{\mathrm{N}}$ at $f_{(-)}$ for $\beta<0$ is larger than the RHCP radiation field component at $f_{(+)}$ for $\beta>0$, when $q>0.147$: $G_{\mathrm{LHCP}}>G_{\mathrm{RHCP}}$. In other words, the gain characteristic for $\mathbf{E}_{\mathrm{C}}$ is the opposite of that for $\mathbf{E}_{\mathrm{N}}$. This fact suggests that an inference can be made: the sum of $\mathbf{E}_{\mathrm{C}}$ and $\mathbf{E}_{\mathrm{N}}$ for $\beta<0$ and for $\beta>0$ will be balanced when an N-type current is distributed across a certain region of the loop and a C-type current is distributed across the remaining region. Thus, it is expected that the unbalanced gain for the N-type metaloop antenna of $1\lambda_{\mathrm{g}}$ circumference will become balanced. This expectation is investigated in the following section.

IV. RADIATION IN THE NORMAL DIRECTION FROM A COMPOSITE OF N-TYPE AND C-TYPE CURRENTS

A. E_{NC} FOR A COMPOSITE CURRENT

To confirm the inference and expectation in Section III, we consider a situation where the N-type current $\mathbf{I}_{\mathrm{N}}(s')$ of Eq. (1) is distributed across a certain region of a loop of one guided wavelength ($|n|=1$) and the C-type current $\mathbf{I}_{\mathrm{C}}(s')$ of Eq. (21) is distributed along the remainder of the loop without overlapping with the N-type current, as shown in Fig. 5:

$$N_{\mathrm{s}} \le \phi' \le N_{\mathrm{e}}\ [\mathrm{rad}] \quad \text{for } \mathbf{I}_{\mathrm{N}}(s') \tag{31}$$

$$C_{\mathrm{s}} \le \phi' \le C_{\mathrm{e}}\ [\mathrm{rad}] \quad \text{for } \mathbf{I}_{\mathrm{C}}(s'), \tag{32}$$

where $N_{\mathrm{s}}=C_{\mathrm{e}}$. This section focuses on the total radiation field in the normal direction, $\mathbf{E}_{\mathrm{N}}+\mathbf{E}_{\mathrm{C}}\equiv\mathbf{E}_{\mathrm{NC}}$, generated from the composite current in Eqs. (31) and (32), denoted as $\mathbf{I}_{\mathrm{NC}}$. An antenna fabricated based on composite current $\mathbf{I}_{\mathrm{NC}}$, called the *NC*-type metaloop antenna, appears later in Section V.

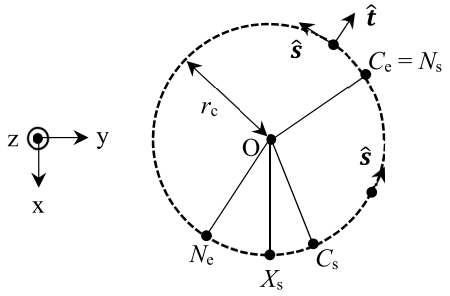

FIGURE 5. Composite of *N*-type and *C*-type currents.

Making use of the results in Sections II and III, we have

$$\mathbf{E}_{\mathrm{NC}}(r,\theta=0,\phi) = Uf_{(-)}[\{\frac{1+q}{2}\cdot(N_{\mathrm{e}}-N_{\mathrm{s}})+\frac{1}{2}\cdot(C_{\mathrm{e}}-C_{\mathrm{s}})\}\mathbf{L} + \{\frac{1-q}{2}\cdot\frac{e^{j2N_{\mathrm{e}}}-e^{j2N_{\mathrm{s}}}}{j2}+\frac{1}{2}\cdot\frac{e^{j2C_{\mathrm{e}}}-e^{j2C_{\mathrm{s}}}}{j2}\}\mathbf{R}] \quad \text{for } n=-1 \tag{33}$$

and

$$\mathbf{E}_{\mathrm{NC}}(r,\theta=0,\phi) = Uf_{(+)}[\{\frac{1+q}{2}\cdot\frac{e^{-j2N_{\mathrm{e}}}-e^{-j2N_{\mathrm{s}}}}{-j2}+\frac{1}{2}\cdot\frac{e^{-j2C_{\mathrm{e}}}-e^{-j2C_{\mathrm{s}}}}{-j2}\}\mathbf{L} + \{\frac{1-q}{2}\cdot(N_{\mathrm{e}}-N_{\mathrm{s}})+\frac{1}{2}\cdot(C_{\mathrm{e}}-C_{\mathrm{s}})\}\mathbf{R}] \quad \text{for } n=+1, \tag{34}$$

where $\mathbf{L}=-j\hat{x}+\hat{y}$ and $\mathbf{R}=j\hat{x}+\hat{y}$. Eqs. (33) and (34) are referred to as $\mathbf{E}_{\mathrm{NC}}^{(-)}$ and $\mathbf{E}_{\mathrm{NC}}^{(+)}$, respectively.

$\mathbf{E}_{\mathrm{NC}}^{(-)}$ and $\mathbf{E}_{\mathrm{NC}}^{(+)}$ for $(C_{\mathrm{s}}, N_{\mathrm{s}}, N_{\mathrm{e}}) = (0, \text{varied}, 2\pi)$ [rad] are illustrated in Fig. 6 and 7, respectively, as a function of N_{s} ($=C_{\mathrm{e}}$) [rad], with polarization factor q as a parameter, where N_{s} is called the boundary azimuth angle of the N-type and C-type currents. As boundary azimuth angle N_{s} is increased, the LHCP radiation field component of $\mathbf{E}_{\mathrm{NC}}^{(-)}$, denoted as ENC(−) LHCP, decreases, as shown in Fig. 6; conversely, the RHCP radiation field component of $\mathbf{E}_{\mathrm{NC}}^{(+)}$, denoted as ENC(+) RHCP, increases, as shown in Fig. 7. Note that the RHCP radiation field component of $\mathbf{E}_{\mathrm{NC}}^{(-)}$, denoted as ENC(−) RHCP, is less than −20 dB and does not appear at the scale of Fig. 6.

Further investigation of Eqs. (33) and (34) for $(C_{\mathrm{s}}, N_{\mathrm{s}}, N_{\mathrm{e}}) = (0, \text{varied}, 2\pi)$ [rad] brings important results when the boundary azimuth angle is $N_{\mathrm{s}}=C_{\mathrm{e}}=\pi$ [rad]. Eqs. (33) and (34) become Eqs. (35) and (36), respectively:

$$\mathbf{E}_{\mathrm{NC}}^{(-)}(r,\theta=0,\phi) = Uf_{(-)}(\frac{1+q}{2}\pi+\frac{1}{2}\pi)\mathbf{L} \quad \text{for } n=-1 \text{ and } (C_{\mathrm{s}}, N_{\mathrm{s}}, N_{\mathrm{e}}) = (0, \pi, 2\pi) \tag{35}$$

$$\mathbf{E}_{\mathrm{NC}}^{(+)}(r,\theta=0,\phi) = Uf_{(+)}(\frac{1-q}{2}\pi+\frac{1}{2}\pi)\mathbf{R} \quad \text{for } n=+1 \text{ and } (C_{\mathrm{s}}, N_{\mathrm{s}}, N_{\mathrm{e}}) = (0, \pi, 2\pi). \tag{36}$$

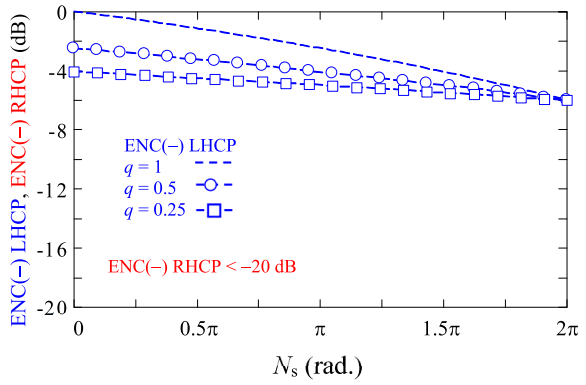

FIGURE 6. Radiation field $\mathbf{E}_{\mathrm{NC}}(r, \theta = 0, \phi)$ for $n = -1$, denoted as $\mathbf{E}_{\mathrm{NC}}^{(-)}$, as a function of boundary angle $N_{\mathrm{s}} = C_{\mathrm{e}}$ with polarization factor q, where $(C_{\mathrm{s}}, N_{\mathrm{e}}) = (0, 2\pi)$ and $f = f_{(-)}$. Note that the RHCP radiation field component of $\mathbf{E}_{\mathrm{NC}}^{(-)}$, ENC(−) RHCP, is less than −20 dB and does not appear at this scale.

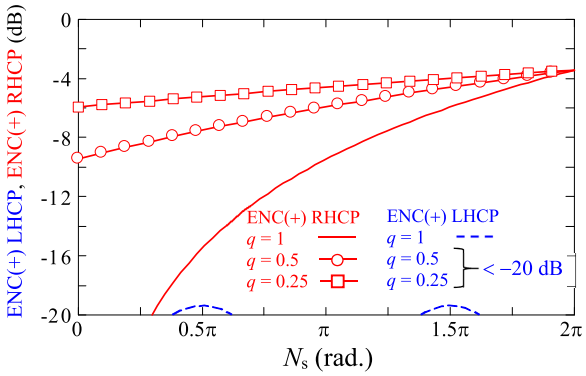

FIGURE 7. Radiation field $\mathbf{E}_{\mathrm{NC}}(r, \theta = 0, \phi)$ for $n = +1$, denoted as $\mathbf{E}_{\mathrm{NC}}^{(+)}$, as a function of boundary angle $N_{\mathrm{s}} = C_{\mathrm{e}}$ with polarization factor q, where $(C_{\mathrm{s}}, N_{\mathrm{e}}) = (0, 2\pi)$ and $f = f_{(+)}$. Note that the LHCP radiation field component of $\mathbf{E}_{\mathrm{NC}}^{(+)}$, ENC(+) LHCP, for $q = 0.5$ and $q = 0.25$ is less than −20 dB and does not appear at this scale.

The above two equations show that, when the loop circumference is one guided wavelength, *i.e.*, $|n| = 1$, the total radiation field is purely LHCP at $f_{(-)}$ and purely RHCP at $f_{(+)}$.

B. BOUNDARY AZIMUTH ANGLE N_s (= C_e)

The $\mathbf{E}_{\mathrm{NC}}$ of Eq. (33) can be approximated by the LHCP radiation field component, as seen from Fig. 6, and the $\mathbf{E}_{\mathrm{NC}}$ of Eq. (34) can be approximated by the RHCP radiation field component, as seen from Fig. 7. Hence, the ratio of the gain at $f_{(-)}$ to the gain at $f_{(+)}$, G_{r}, is

$$G_{\mathrm{r}} = \frac{\left| f_{(-)} \left\{ \frac{1+q}{2} (2\pi - N_{\mathrm{s}}) + \frac{1}{2} N_{\mathrm{s}} \right\} \right|^2}{\left| f_{(+)} \left\{ \frac{1-q}{2} (2\pi - N_{\mathrm{s}}) + \frac{1}{2} N_{\mathrm{s}} \right\} \right|^2}$$
$$\text{for } |n| = 1 \text{ and } (C_{\mathrm{s}}, N_{\mathrm{s}}, N_{\mathrm{e}}) = (0, \text{varied}, 2\pi)\,. \quad (37)$$

Fig. 8 shows the gain ratio of Eq. (37) as a function of boundary azimuth angle N_{s} with polarization factor q as a parameter. This figure is used to determine boundary azimuth angle N_{s} for the gain ratio at a specified value of q.

Our requirement in this paper is to obtain balanced gain: $G_{\mathrm{r}} = 1$, *i.e.*, $G_{\mathrm{r}} = 0$ [dB] in Fig. 8. The boundary angle that must be determined is given by the intersection of the line for $G_{\mathrm{r}} = 0$ dB with the line for the specified q.

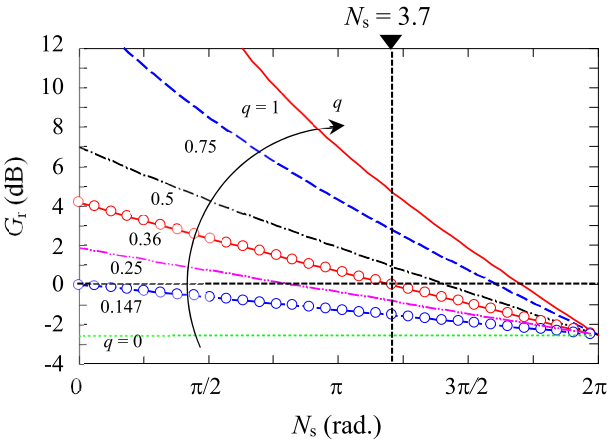

FIGURE 8. Gain ratio as a function of boundary angle N_{s} with polarization factor q as a parameter.

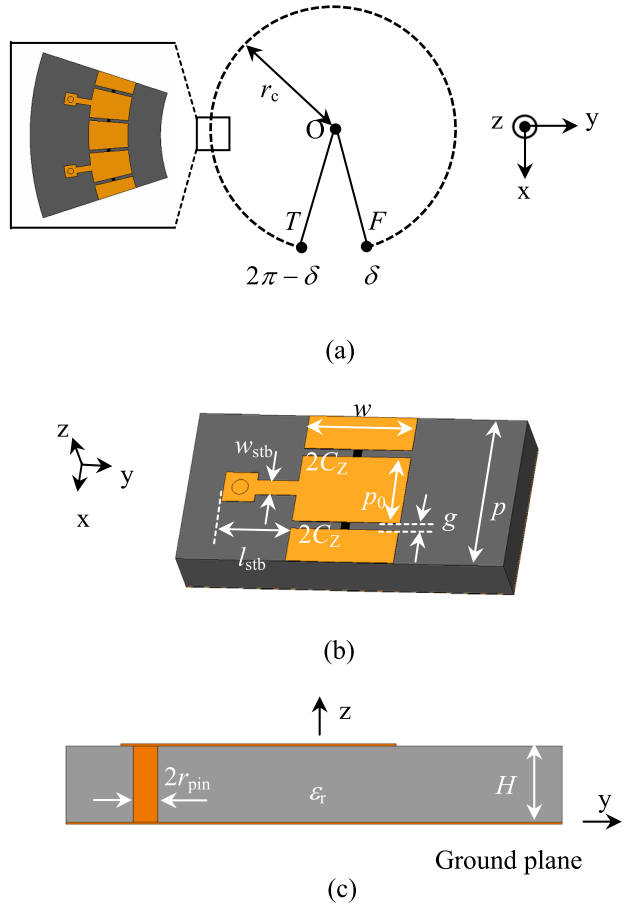

FIGURE 9. Simulation model for an *N*-type metaloop antenna composed of *N*-type metaatoms, where $(N_{\mathrm{s}}, N_{\mathrm{e}}) = (\delta, 2\pi - \delta)$ with $\delta = 0.05\pi$ [rad]. (a) Schematic drawing. See also Fig. 14. (b) Perspective view of the *N*-type metaatom. (c) Side view of the *N*-type metaatom.

V. SIMULATION AND ANTENNA FABRICATION USING N-TYPE AND C-TYPE METAATOMS

The preliminary discussions in Sections II through IV have been made without referring to the practical elements that

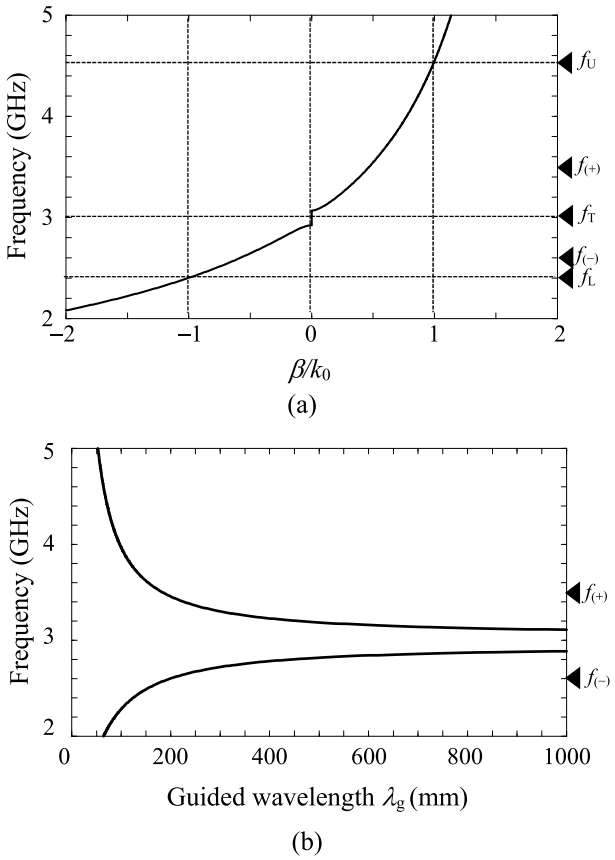

FIGURE 10. Dispersion of an *N*-type metaatom. (a) Frequency – (β/k_0). (b) Frequency – λ_g.

produce the N-type and C-type currents. The discussion in this section is performed by introducing these elements, called the N-type and C-type metaatoms [28].

A. SIMULATION MODEL

Fig. 9(a) shows the simulation model for an N-type metaloop antenna composed of numerous N-type metaatoms printed on a grounded substrate of radius $R_{GP} = 55$ mm. Figs. 9(b) and (c) elaborate the N-type metaatom. The array of N-type metaatoms occupies a region of $\delta \leq \phi' \leq 2\pi - \delta$ [rad] with $\delta = 0.05\pi$ [rad]. The loop radius is $r_c = 200/2\pi$ mm. Point F is the feed point and point T is the loop end terminated to a ground plane through a resistive load (Bloch impedance $R_B = 60$ ohms). This antenna simulation model has an unbalanced gain and is modified to a new antenna simulation model with a balanced gain using C-type metaatoms.

The dispersion of the metaatom in Figs. 9(b) and (c) is shown in Fig. 10, which is designed using an EM simulator [29] such that transition frequency f_T is 3 GHz, $f_{(-)} = 2.6$ GHz, and $f_{(+)} = 3.5$ GHz. The parameters used here are as follows [27]. H (=3.2 mm) and ε_r (=2.6) are, respectively, the thickness and relative permittivity of the grounded dielectric substrate; $2C_Z$ (=1.2 pF) is the capacitance of the chip capacitor inserted into gap g (=0.5 mm) between neighboring conducting strips of width w (=6.6 mm); and p (=$2p_0$+ $2g$ = 10 mm) is the length

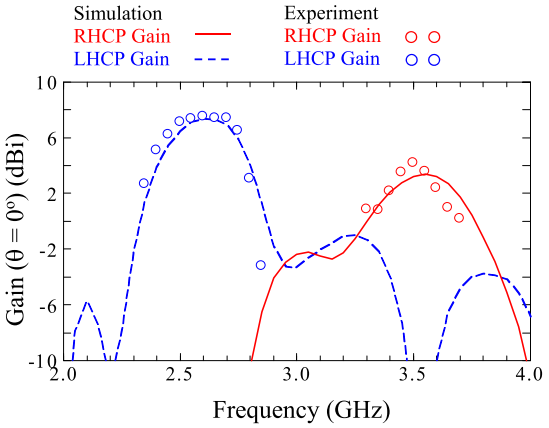

FIGURE 11. Frequency response of the gain for the *N*-type metaloop antenna, where $(N_s, N_e) = (\delta, 2\pi - \delta)$ with $\delta = 0.05\pi$ [rad].

of the metaatom (periodicity). Other parameters l_{stb} and w_{stb} are the respective length and width of the stub, which is short-circuited to the ground plane through a conducting pin of diameter $2r_{pin}$: (l_{stb}, w_{stb}, $2r_{pin}$) = (4.5 mm, 1.0 mm, 1.0 mm).

Frequencies f_L and f_U in Fig. 10 are the lower- and upper-band edge frequencies for a fast wave, respectively. The propagation phase constant is negative ($\beta < 0$) below f_T and positive ($\beta > 0$) above f_T. Frequency $f_{(-)} = 2.6$ GHz and $f_{(+)} = 3.5$ GHz, where the guided wavelength normalizes the loop circumference of $2\pi r_c$, lead to a frequency ratio of $f_r = f_{(-)}/f_{(+)} = 0.743$, which has already been used in the preliminary discussions.

Fig. 11 shows the frequency response of the gain for the N-type metaloop antenna simulation model in Fig. 9. In accordance with the theoretical results in Section II, the maximum LHCP gain is obtained near $f_{(-)} = 2.6$ GHz and the maximum RHCP gain is obtained near $f_{(+)} = 3.5$ GHz. The unbalanced gains at these two frequencies lead to a gain ratio of $G_r = 4.1$ dB. Applying this gain ratio to Eq. (37), the polarization factor is determined to be $q = 0.36$.

Next, we change the unbalanced gain shown in Fig. 11 to a balanced gain. For this, we modify the original N-type metaloop antenna simulation model in Fig. 9 into an NC-type metaloop antenna simulation model by introducing C-type metaatoms [22], as shown in Fig. 12. The C-type metaatoms occupy the region $\delta \leq \phi' \leq C_e$ [rad] and produce C-type current, followed by N-type current produced by N-type metaatoms occupying the remaining region of $N_s \leq \phi' \leq (2\pi - \delta)$ [rad], with $N_s = C_e$.

The dispersion of the C-type metaatom is designed to be as similar as possible to that of the N-type metaatom, as shown in Fig. 13, where the center strip is connected through a chip inductor of L_Y (=1.8 nH) to the ground plane by a conducting pin of diameter $2r_{pin}$ (=1.0 mm) as shown in Figs. 13(b) and (c). The configuration parameters for the C-type metaatom, (H, ε_r $2C_Z$, g, w, p), are the same as those of the N-type metaatom.

Gain balance occurs when the gain ratio is 1, *i.e.*, $G_r = 0$ [dB] in Fig. 8. Hence, we search for the intersection

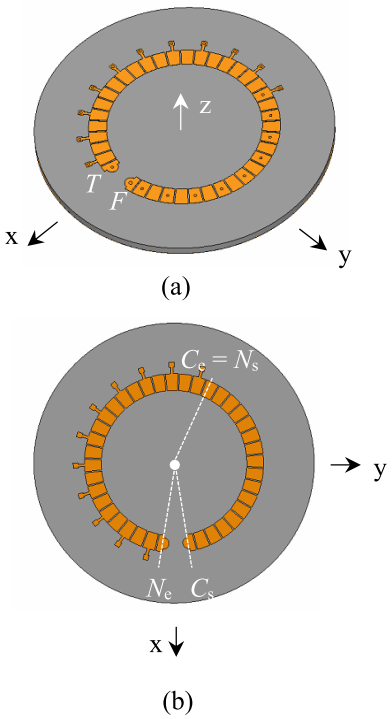

FIGURE 12. Modified *N*-type metaloop antenna (*NC*-type metaloop antenna) simulation model composed of *N*-type metaatoms distributed across region (N_s, N_e) = (N_s, $2\pi - \delta$) and *C*-type metaatoms distributed across region (C_s, C_e) = (δ, N_s), where $\delta = 0.05\pi$ [rad]. Angle N_s (= C_e) is the boundary azimuth angle. (a) Perspective view. (b) Top view.

of the $G_r = 0$ dB line with the $q = 0.36$ (already obtained value) line. The intersection indicates a boundary azimuth angle of N_s (=C_e) $= 1.18\pi$ [rad]. Thus, all details required for modifying the *N*-type metaloop antenna are known.

A comment is made here: an angle of $\delta = 0.05\pi$ [rad] is used for fabrication of a practical *NC*-type metaloop antenna, which appears in subsection *B* below. The effect on the gain caused by using this small angle is almost insignificant. The gain for (N_s, N_e) = (δ, $2\pi - \delta$) is very close to the gain for (N_s, N_e) = (0, 2π), and hence can be approximated by the gain for (N_s, N_e) = (0, 2π) with negligible error.

B. FABRICATION OF AN NC-TYPE METALOOP ANTENNA

Based on the simulation results in subsection *A* above, first, an *N*-type metaloop antenna with (N_s, N_e) = (δ, $2\pi - \delta$) where $\delta = 0.05\pi$ [rad] is fabricated, as shown in Fig. 14. The measured gain is presented in Fig. 11, with good agreement with the simulated gain, which indirectly validates the value of the polarization factor, $q = 0.36$. It is clear that the LHCP gain at $f_{(-)}$ and RHCP gain at $f_{(+)}$ are unbalanced at this phase.

Next, the *N*-type metaloop antenna is modified into an *NC*-type metaloop antenna, as shown in Fig. 15. Both the *N*-type and *C*-type metaatoms have a periodicity of $p = 10$ mm. The number of *N*-type and *C*-type metaatoms is chosen to be 8 and 11, respectively, leading to a boundary azimuth angle of $N_s = 1.15\pi$ [rad], which is very close to the theoretical

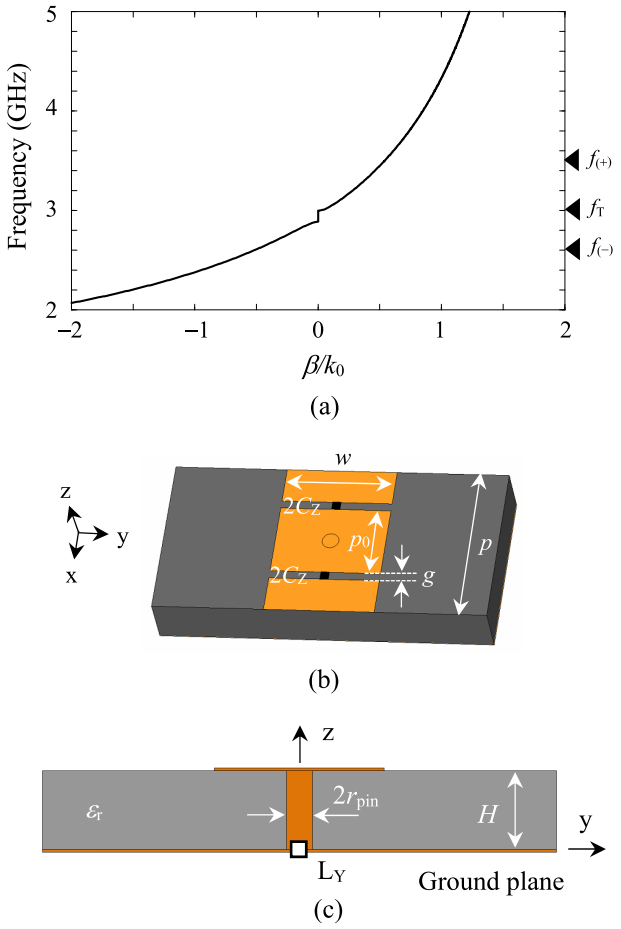

FIGURE 13. *C*-type metaatom. (a) Dispersion. (b) Perspective view of the *C*-type metaatom. (c) Side view of the *C*-type metaatom.

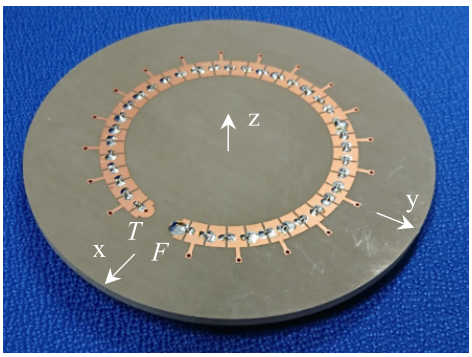

FIGURE 14. Fabricated *N*-type metaloop antenna.

value of $N_s = 1.18\pi$ [rad] obtained in subsection *A* of this section.

Fig. 16 shows the frequency response of the simulated and measured gains for the *NC*-type metaloop antenna. In accordance with the theoretical results in Section IV, the maximum LHCP gain at $f_{(-)}$ is balanced with respect to the maximum RHCP gain at $f_{(+)}$, with good agreement of the simulated and measured results. Thus, the theoretical determination of boundary azimuth angle N_S is validated.

Note that the gain simulation is performed using lossless lump capacitors. There is no remarkable difference between

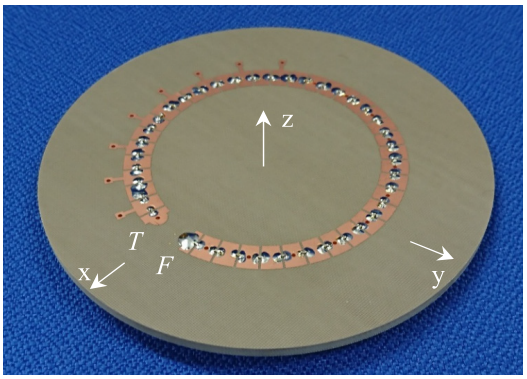

FIGURE 15. Fabricated *NC*-type metaloop antenna.

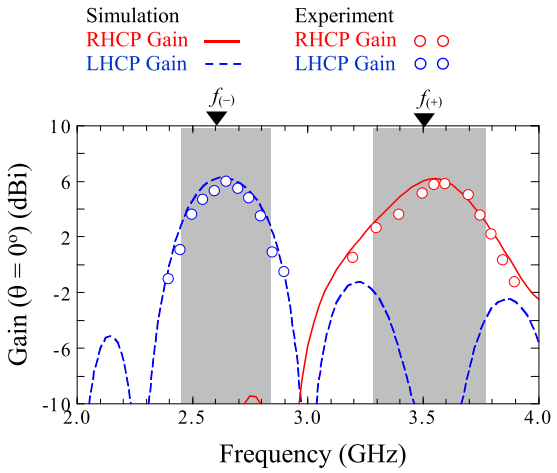

FIGURE 16. Frequency response of the gain for the *NC*-type metaloop antenna. The shadowed regions show the 3-dB gain bandwidth region.

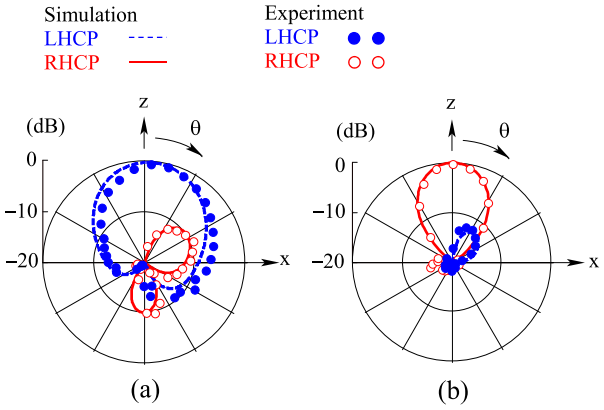

FIGURE 17. Radiation pattern for the *NC*-type metaloop antenna. (a) At $f_{(-)}$. (b) At $f_{(+)}$.

the simulated and measured results. This means that the lump capacitors used are close to lossless capacitors and the effect of the lump capacitors on the radiation efficiency is insignificant.

The other antenna characteristics for the balanced-gain *NC*-type metaloop antenna are summarized as follows: the 3-dB gain bandwidth around $f_{(-)}$ is 13.8% and that around

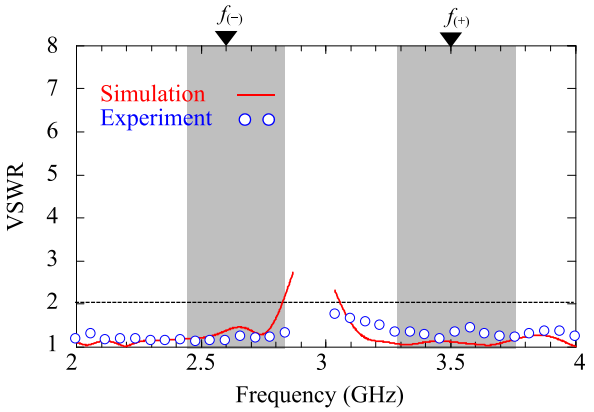

FIGURE 18. Frequency response of the VSWR for the *NC*-type metaloop antenna. The shadowed regions show the 3-dB gain bandwidth region.

$f_{(+)}$ is 13.9%; the radiation pattern shows good agreement between the simulated and measured results, with an axial ratio of less than 3 dB in the normal direction, as shown in Fig. 17; and the VSWR across the gain bandwidth around $f_{(-)}$ and $f_{(+)}$ is desirably small: less than two, as shown in Fig. 18.

It is worth mentioning that the *NC*-type metaloop antenna is terminated through a resistive load (Bloch resistance) to the ground plane at point T, thereby absorbing the current that reaches point T (called the remaining current) and eliminating/suppressing reflection currents from point T toward feed point F. This makes the VSWR small in an almost frequency-independent manner, although the radiation efficiency is reduced (82% at $f_{(-)}$ and 37% at $f_{(+)}$). In contrast, the gain bandwidth is frequency-dependent. This is due to the fact that the gain has the maximum value when the antenna circumference is electrically one-guided wavelength. As the antenna circumference electrically deviates from one-guided wavelength, *i.e.*, as frequency deviates from $f_{(-)}$ and $f_{(+)}$, the gain decreases, resulting in a finite gain bandwidth.

VI. CONCLUSIONS

Balanced radiation for a metaloop antenna with dual-band (Du-BND) counter circularly polarized (Cnt-CP) radiation capability has been theoretically realized through the following five steps. First, the radiation field in the normal direction (z-direction) generated from an N-type current flowing along a loop with propagation phase constant β (positive or negative), $\mathbf{E}_{\mathrm{N}}$, is formulated, where the N-type current is specified by polarization factor q ($0 \leq q \leq 1$). It is found that, when the loop has one guided wavelength ($1\lambda_{\mathrm{g}}$) circumference, a Du-BND Cnt-CP radiation characteristic is obtained, except when $q = 1$. However, the intensity of the left-handed circularly polarized (LHCP) component of $\mathbf{E}_{\mathrm{N}}$ at low frequency $f_{(-)}$ and the intensity of the right-handed circularly polarized (RHCP) component of $\mathbf{E}_{\mathrm{N}}$ at high frequency $f_{(+)}$ are unbalanced, except at a particular value of q.

In preparation for resolving the unbalanced intensities of $\mathbf{E}_{\mathrm{N}}$ (and hence the unbalanced gains) at $f_{(-)}$ and $f_{(+)}$,

secondly, the radiation field generated from a C-type current, $\mathbf{E}_{\mathrm{C}}$, is formulated. From an insight into the characteristics of $\mathbf{E}_{\mathrm{C}}$ and $\mathbf{E}_{\mathrm{N}}$, it is inferred that the unbalance will be resolved when the N-type current on a certain region of the loop is replaced by a C-type current. Based on this inference, thirdly, the radiation field generated from a composite of the N-type and C-type currents, $\mathbf{E}_{\mathrm{NC}}$, is formulated. It is found that a balanced gain is obtained when the boundary azimuth angle of the N-type and C-type currents, N_{s}, is appropriately chosen.

The above-mentioned discussions for $\mathbf{E}_{\mathrm{N}}$, $\mathbf{E}_{\mathrm{C}}$, and $\mathbf{E}_{\mathrm{NC}}$, called the preliminary discussions, do not refer to any practical elements that produce the N-type and C-type currents. In the light of this fact, fourthly, using practical N-type metaatoms for the N-type current and practical C-type metaatoms for the C-type current, two simulation models are created for the N-type and NC-type metaloop antennas. The gain of the N-type metaloop antenna simulation model composed entirely of N-type metaatoms provides supporting information for the determination of polarization factor q. Using the formula for the gain ratio, G_{r}, derived in the preliminary discussions together with the supporting information, the unknown value for q in the N-type metaloop antenna simulation model is successfully determined. Subsequently, this q value is applied to the G_{r}-N_{s} chart made in the preliminary discussions, to obtain the boundary azimuth angle, N_{s}, for which the NC-type metaloop antenna simulation model will realize a balanced gain.

Finally, the NC-type metaloop antenna simulation model is realized by fabricating a practical antenna. The validity of the design process toward balancing the gain is confirmed by showing good agreement of the simulated and measured gains. The gain bandwidth, radiation pattern, and VSWR of the fabricated NC-type metaloop antenna are also presented.

ACKNOWLEDGMENT

The authors would like to thank V. Shkawrytko for his assistance in the preparation of this manuscript. They would also like to thank Junya Miyake, Kenta Yoshida, Tomohiro Yoshida, Kazutoshi Sakata, and Ittoku Yoshino for their contribution to the research on metaatoms and metaloop antennas.

REFERENCES

[1] L. Shafai, S. K. Sharma, and S. Rao, Eds., *Handbook of Reflector Antennas and Feed Systems Volume II: Feed Systems*. Boston, MA, USA: Artech House, Jul. 2013.
[2] Z. Chen, D. Liu, H. Nakano, X. Qing, and T. Zwick, Eds., *Handbook of Antenna Technologies*. Singapore: Springer, 2016.
[3] J. D. Kraus and R. J. Marhefka, *Antennas*, 3rd ed. New York, NY, USA: McGraw-Hill, 2002, ch. 8.
[4] X. Tang, Y. He, and B. Feng, "Design of a wideband circularly polarized strip-helical antenna with a parasitic patch," *IEEE Access*, vol. 4, pp. 7728–7735, 2016.
[5] J. Dinkić, D. Olćan, A. Djordjević, and A. Zajić, "Design and optimization of nonuniform helical antennas with linearly varying geometrical parameters," *IEEE Access*, vol. 7, pp. 136855–136866 2019.
[6] H. Nakano and J. Yamauchi, "The balanced helices radiating in the axial mode," in *Proc. Antennas Propag. Soc. Int. Symp.*, Seattle, WA, USA, Jun. 1979, Art. no. 404407.
[7] J. A. Kaiser, "The Archimedean two-wire spiral antenna," *IRE Trans. Antennas Propag.*, vol. 8, no. 3, pp. 312–323, May 1960.
[8] H. Nakano, K. Nogami, S. Arai, H. Mimaki, and J. Yamauchi, "A spiral antenna backed by a conducting plane reflector," *IEEE Trans. Antennas Propag.*, vol. 34, no. 6, pp. 791–796, Jun. 1986.
[9] G. Li, G. Gao, W. Liu, and Z. Tian, "Tunable and flexible liquid spiral antennas," *Electron. Lett.*, vol. 53, no. 10, pp. 648–650, May 2017.
[10] H. Nakano, S. Okuzawa, K. Ohishi, H. Mimaki, and J. Yamauchi, "A curl antenna," *IEEE Trans. Antennas Propag.*, vol. 41, no. 11, pp. 1570–1575, Nov. 1993.
[11] S. M. O'Kane and V. F. Fusco, "Circularly polarized curl antenna lens with manual tilt properties," *IEEE Trans. Antennas Propag.*, vol. 57, no. 12, pp. 3984–3987, Dec. 2009.
[12] C. Zhang, J. Shi, and Q. Cao, "A low-profile curl antenna with parasitic curl," in *Proc. IEEE 5th Asia–Pacific Conf. Antennas Propag. (APCAP)*, Kaohsiung, Taiwan, Jul. 2016, p. 139.
[13] P. J. Massey, P. Fellows, D. Mirshekar-Syahkal, A. Pal, and A. Mehta, "Loop antennas," in *Handbook of Antenna Technologies*, vol. 2. Springer, 2016, pp. 723–786.
[14] J. Liu, Z. Tang, Z. Wang, H. Li, and Y. Yin, "Gain enhancement of a broadband symmetrical dual-loop antenna using shorting pins," *IEEE Antennas Wireless Propag. Lett.*, vol. 17, no. 8, pp. 1369–1372, Aug. 2018.
[15] H. Nakano, "A numerical approach to line antennas printed on dielectric materials," in *Computer Physics Communications*, vol. 68. Amsterdam, The Netherlands: North Holland, Aug. 1991, pp. 441–450.
[16] H. Nakano, "Circularly polarized loop antenna," Japan Patent 03 431 045, May 23, 2003.
[17] H. Nakano, T. Abe, A. Mehta, and J. Yamauchi, "Circularly polarized concentric metaring antenna," in *Proc. EuCAP*, vol. 4. Copenhagen, Denmark, Mar. 2020, pp. 1–4.
[18] C. Caloz and T. Itoh, *Electromagnetic Metamaterials*. Hoboken, NJ, USA: Wiley, 2006.
[19] G. Eleftheriades and K. Balmain, *Negative-Refraction Metamaterials: Fundamental Principles and Applications*. Hoboken, NJ, USA: Wiley, 2005.
[20] N. Engheta and R. W. Ziolkowski, *Electromagnetic Metamaterials: Physics and Engineering Explorations*. Hoboken, NJ, USA: Wiley, 2006.
[21] H. Nakano, *Low-Profile Natural and Metamaterial Antennas*. Hoboken, NJ, USA: Wiley, 2016.
[22] H. Nakano, K. Yoshida, and J. Yamauchi, "Radiation characteristics of a metaloop antenna," *IEEE Antennas Wireless Propag. Lett.*, vol. 12, pp. 861–863, 2013.
[23] H. Nakano, T. Yoshida, and J. Yamauchi, "Triband metaloop antenna," *IEEE Antennas Wireless Propag. Lett.*, vol. 16, pp. 1981–1984, 2017.
[24] H. Nakano, T. Abe, J. Yamauchi, and A. Mehta, "Double metaloop antenna," in *Proc. IEEE Int. Symp. Antennas Propag. USNC-URSI Radio Sci. Meeting*, Atlanta, GA, USA, Jul. 2019, pp. 1591–1592.
[25] H. Nakano, T. Abe, and J. Yamauchi, "Metaline application to loop antennas," in *Proc. Int. Workshop Antenna Technol. (iWAT)*, Miami, FL, USA, Mar. 2019, pp. 157–158.
[26] H. Nakano, I. Yoshino, T. Abe, and J. Yamauchi, "Balanced gain for a square metaloop antenna," *EPJ Appl. Metamater.*, vol. 6, no. 1, pp. 1–5, Jan. 2019.
[27] H. Nakano, T. Abe, and J. Yamauchi, "Quasi-theoretical investigation of four circularly polarized metaloop antennas," *EPJ Appl. Metamater.*, vol. 6, no. 2, pp. 1–13, Jan. 2019.
[28] H. Nakano, T. Abe, A. Mehta, and J. Yamauchi, "Application of a circularly polarized metaline to beam-steerable antennas," in *Proc. 12th Eur. Conf. Antennas Propag. (EuCAP)*, London, U.K., 2018.
[29] *CST Computer Simulation Technology GmbH*, Darmstadt, Germany, Microwave Studio. Accessed: May 2020. [Online]. Available: http://www.cst.com

HISAMATSU NAKANO (Life Fellow, IEEE) has held positions as a Visiting Associate Professor with Syracuse University, from March 1981 to September 1981, and a Visiting Professor with the University of Manitoba, from March 1986 to September 1986, the University of California at Los Angeles, from September 1986 to March 1987, and Swansea University, U.K., from July 2016 to September 2019. He has been with Hosei University, since 1973, where he is currently a Professor Emeritus and a Special-Appointment Researcher with the Electromagnetic Wave Engineering Research Institute attached to the Graduate School. He has published over 330 articles in peer-reviewed journals and 11 books/book chapters, including the *Low-Profile Natural and Metamaterial Antennas* (IEEE Press, Wiley, 2016). His significant contributions are the development of five integral equations for line antennas in free space and printed on a dielectric substrate, the invention of an L-shaped wire/strip antenna feeding method, and the realization of numerous wideband antennas, including curl, metaspiral, metahelical, and body of revolution antennas. His other accomplishments include design of antennas for GPS, personal handy phones, space radio, electronic toll collection, RFID, UWB, and radar. He has been awarded 78 patents, including Curl Antenna Element and Its Array, Japan. His research interests include numerical methods for low- and high-frequency antennas and optical waveguides. He has served as a member of the IEEE APS Administrative Committee, from 2000 to 2002, and a Region 10 Representative, from 2001 to 2010. He received the H. A. Wheeler Award, in 1994, the Chen-To Tai Distinguished Educator Award, in 2006, and the Distinguished Achievement Award, in 2016, all from the IEEE Antennas and Propagation Society. He was also a recipient of The Prize for Science and Technology from the Japan's Minister of Education, Culture, Sports, Science and Technology, in 2010. Most recently, he was selected as a recipient of the Antenna Award of the European Association on Antennas and Propagation (EurAAP), in 2020. He is an Associate Editor of several scientific journals and magazines, such as *Electromagnetics* and the *IEEE Antennas and Propagation Magazine*.

TOMOKI ABE (Member, IEEE) was born in Miyagi, Japan, in August 1994. He received the B.E. and M.E. degrees in electronics and electrical engineering from Hosei University, Tokyo, Japan, in 2017 and 2019, respectively. He is currently a member of the Institute of Electronics, Information and Communication Engineers, Japan.

JUNJI YAMAUCHI (Life Fellow, IEEE) was born in Nagoya, Japan, in August 1953. He received the B.E., M.E., and Dr.E. degrees from Hosei University, Tokyo, Japan, in 1976, 1978, and 1982, respectively. From 1984 to 1988, he has served as a Lecturer with the Electrical Engineering Department, Tokyo Metropolitan Technical College. Since 1988, he has been a member of the faculty of Hosei University, where he is currently a Professor with the Electrical and Electronic Engineering Department. He is the author of the *Propagating Beam Analysis of Optical Waveguides* (Research Studies Press, 2003). His research interests include optical waveguides, polarization converters, and circularly polarized antennas. He is a member of the Optical Society of America and the Institute of Electronics, Information and Communication Engineers, Japan.